CLAY BARRIERS ASSESSMENT: A COUPLED MECHANICAL AND MOISTURE TRANSFER MODEL

F. Collin, X.L. Li, J. -P. Radu and R. Charlier

MSM Department
University of Liege, Belgium
Member of the ALERT GEOMATERIALS network

Key words: Geomechanics, thermo-hydro-mechanical coupling, unsaturated soils.

Abstract. *A thermo-hydro-mechanical model is presented to tackle the complex coupling problems encountered in clay barriers. A detailed formulation coupling heat, moisture (liquid water and water vapour) and air transfer in a deformable unsaturated soil is given. The formulation of Alonso-Gens's mechanical model for unsaturated soil is also incorporated. The sensitivity to some parameters and their determinations are analysed. Finally, a small scale wetting – heating test on compacted bentonite is performed for validation; the numerical results are compared to the experimental measurements.*

1. Introduction

Some nuclear waste disposal concepts are based on the waste storage in deep clay geological layers. The nuclear canisters are surrounded by highly compacted clay, which undergoes initially a very high suction (up to 100 MPa or more) and this suction modifies the hydro-mechanical behaviour. Moreover the confinement barrier is subject to high temperature (over 70°C and sometimes over 100°C). A good design of a clay barrier should take all these phenomena into account. For this purpose, constitutive laws have been developed. They are coupling water flow, heat flow and soil mechanic. They have been implemented in a finite element code, which allows analysing non-homogenous transient problems.

The mechanical behaviour of an unsaturated soil depends of stress level and of suction. A refined model has been proposed ten years ago by Alonso and Gens. On the other hand, the water flow in unsaturated media is a non-linear problem, which has been extensively discussed by Thomas [1]. Moreover high temperature induces the production of water vapour (which depends also on the suction level). Its modelling is based on Philip and De Vries's contribution.

The developed finite elements are based on the following degrees of freedom: soil skeleton displacements, temperature, liquid water pressure, and gas (dry air + vapour) pressure. The elements have a monolithically form, and all coupling terms in the Newton-Raphson's stiffness matrix are taken into account, allowing a good convergence rate for most treated problems.

A validation of the constitutive laws and of the finite element code is obtained thanks to a comparison with other code results and with some experimental results.

2. Diffusion model

In clay barriers, unsaturated conditions and thermal variations create several coupling effects that influence the design of each component of the barriers. Moreover high temperatures in unsaturated conditions induce production of water vapour. Thus, gas phase is a mixture of dry air and water vapour. Liquid water and dissolved air compound the liquid phase.

The variables chosen for the description of the flow problem are liquid water pressure, gas pressure and temperature.

2.1 Water species

The mass conservation equation is written for the mass of liquid water and water vapour.

Vapour flows will have significant effects on moisture transfer only if liquid and vapour flows have a same order of magnitude. Clay presents a very low permeability and very slow liquid water motions. So the effect of water vapour transport in this type of soil may not be neglected.

2.1.1 Mass conservation for the water

The equation includes the variation of water storage and the divergence of water flows, including the liquid and vapour effects:

$$\underbrace{\frac{\partial \rho_w n S_{r,w}}{\partial t} + div(\rho_w \underline{f}_w)}_{Liquid\ water} + \underbrace{\frac{\partial \rho_v n S_{r,g}}{\partial t} + div(\rho_v \underline{f}_v + \rho_v \underline{f}_g)}_{Water\ vapour} = 0. \qquad (2.1)$$

Where ρ_α and $\underline{f}_\alpha$ are respectively the density and the macroscopic velocity of the component α; n is medium porosity; $S_{r,w}$ is water saturation degree in volume $S_{r,g}$ is gas saturation degree in volume and t is the time.

Water vapour is one of the gas phase's compounds. Therefore, vapour flows thanks to vapour diffusion in the gaseous phase and to gas convection.

2.1.2 Motion of the liquid water

The generalised Darcy's law for multiphase porous medium gives liquid water velocity:

$$\underline{f}_w = -\frac{k_{int} k_{r,w}}{\mu_w}[\nabla p_w + g\rho_w \nabla y]. \qquad (2.2)$$

Where p_w is the liquid water pressure; y is the vertical, upward directed co-ordinate; g is the gravity acceleration; μ_w is the dynamic viscosity of the liquid water; k_{int} is the intrinsic permeability of the medium and $k_{r,w}$ is the water relative permeability.

The water permeability varies with respect to the saturation degree in unsaturated conditions.

2.1.3 Couplings between the liquid water and other variables

The liquid water properties (i.e. density and viscosity) depend on temperature. This induces a coupling between liquid water flow and thermal flow: some convective water flows can be created due to temperature distribution. Another coupling effect is due to permeability, which depends on suction (i.e. the difference between the gas and water pressure). The suction field will influence the water flows.

2.1.4 Diffusion of water vapour

The water vapour flow is assumed to respect a Fick's diffusion law. The vapour diffusion is linked to a gradient of vapour density:

$$\underline{f}_v = -D\underline{\nabla}\rho_v. \tag{2.3}$$

The water vapour density ρ_v is given by a thermodynamic relation [2]:

$$\rho_v = \rho_0 h. \tag{2.4}$$

Where ρ_0 is the saturated water vapour density and h is the relative humidity.

The Kelvin-Laplace's law gives the relative humidity h:

$$h = \exp\left(\frac{p_w - p_g}{\rho_w R_v T}\right). \tag{2.5}$$

Where R_v is the gas constant of water vapour and T is the temperature.

The relative humidity allows taking into account adsorption phenomena and capillary effect in the soil.
The diffusion coefficient D is not easy to determine. It is supposed to depend on the saturation degree and the tortuosity. Following Philip's and De Vries's model [3], the following relation is assumed:

$$D = \frac{D_{atm}\nu_v\tau_v n S_{r,g}}{\rho_v}. \tag{2.6}$$

Where D_{atm} is the diffusion coefficient of vapour in atmosphere; ν_v is the 'mass flow' factor and τ_v is the tortuosity.

The vapour is considered as a perfect gas, which respects the following law:

$$p_v = \rho_v R_v T. \tag{2.7}$$

The gradient of the water vapour density can now be developed in order to compute the vapour flow:

$$\underline{\nabla}\rho_v = \frac{\rho_0 g h}{R_v T}\underline{\nabla}\frac{p_w - p_g}{\rho_w g} + \left[h\frac{\partial\rho_0}{\partial T} - \frac{\rho_0\left(p_w - p_g\right)h}{\rho_w R_v T^2}\right]\underline{\nabla}T. \tag{2.8}$$

The water vapour density gradient can be separated into two contributions: an isothermal one

related to a suction gradient and a thermal one due to a temperature gradient.

2.1.5 Couplings between the water vapour and other variables

As shown above, the vapour properties and flows depend essentially on temperature and on gas pressure fields. This model can reproduce the vapour transport from the points at high temperature (where the water vapour is produced) to the points at lower temperature (where the water vapour condenses).

2.2 Dry air species

Dry air is a part of a gas mixture: dry air and water vapour compose the gas phase. Dissolved air is also present in the water, its contribution is taken into account in the balance equation. The dry air pressure is not a basic variable: this pressure will be computed up to the gas and the vapour pressure.
Dalton's law is assumed: the pressure of the gas mixture is equal to the sum of the partial pressures, which each gas would exert if it filled alone all the volume considered.

2.2.1 Mass conservation for the dry air

The equation of mass conservation includes the contributions of the dry air phase and of the dissolved air in water:

$$\underbrace{\frac{\partial \rho_a n S_{r,g}}{\partial t} + div(\rho_a \underline{f}_a + \rho_a \underline{f}_g)}_{\text{Dry air in gas phase}} + \underbrace{\frac{\partial H \rho_a n S_{r,w}}{\partial t} + div(H \rho_a \underline{f}_w)}_{\text{Dissolved air in water}} = 0. \tag{2.9}$$

Where ρ_a is dry air density and H is Henry's coefficient.

Henry's coefficient H allows determining the dissolved air in the liquid water. The dissolved air mass is supposed to be sufficiently low in order to consider that the water properties are not influenced. The dry air flow in the gaseous phase is due to the flow of the gas mixture and to the dry air diffusion flow.

2.2.2 Diffusion of dry air

The dry air diffusion flow is related to dry air density gradient. Using the diffusion theory adapted to porous medium, the diffusion dry air flows can be computed by:

$$\underline{f}_a = -\lfloor D_{atm}.\nu_v.\tau_v.\theta_g / \rho_a \rfloor \underline{grad}(\rho_a). \tag{2.10}$$

2.2.3 Motion of gas

The generalised Darcy's law for multiphase medium gives the gas velocity:

$$\underline{f}_g = -\frac{k_{\text{int}} k_{r,g}}{\mu_g}\left[\underline{\nabla} p_g + g\rho_g \underline{\nabla} y\right]. \tag{2.11}$$

Where μ_g is the gas dynamic viscosity; $k_{r,g}$ is the gas relative permeability and ρ_g is the gas density.

The gas permeability is adapted in order to reproduce its variation in non-saturated conditions.

2.3 Heat diffusion

2.3.1 Conservation of the heat

$$\frac{\partial \phi}{\partial t} + div(\underline{q}) - Q = 0. \tag{2.12}$$

Where ϕ is the enthalpy of the medium; $\underline{q}$ is the heat flow and Q is a volume heat source.

2.3.2 Quantity of heat storage: Enthalpy

The enthalpy of the system is given by the sum of each component's enthalpy:

$$\begin{aligned}\phi = {} & nS_{r,w}\rho_w c_{p,w}(T - T_0) + nS_{r,g}\rho_a c_{p,a}(T - T_0) \\ & + (1-n)\rho_s c_{p,s}(T - T_0) + nS_{r,g}\rho_v c_{p,v}(T - T_0) \\ & + nS_{r,g}\rho_v L.\end{aligned} \tag{2.13}$$

Where $c_{p,\alpha}$ is the specific heat of the component α and L is the vaporisation latent heat. The last enthalpy term corresponds to the heat stored during the water vaporisation.

2.3.3 Heat transport

The heat transport is related to the conduction effect, the convection one and the vaporisation one.

$$\underline{q} = -\Gamma \underline{\nabla} T + \left[c_{p,w}\rho_w \underline{f}_w + c_{p,a}\rho_a(\underline{f}_a + \underline{f}_g) + c_{p,v}\rho_v(\underline{f}_v + \underline{f}_g)\right](T - T_0) + \left(\rho_v \underline{f}_v + \rho_v \underline{f}_g\right)L. \tag{2.14}$$

Where Γ is the medium conductivity.

Some authors explicitly model also the solid convection, which is typically a large strains, large displacements effect. Our model takes the large strains and large rotations of the sample into account, thanks to a Lagrangian actualised formulation. Therefore the equilibrium and balance equations, as well as the water, air, and heat flow are expressed in the moving current configuration. This implies that the solid convection effect is implicitly taken into account.

2.3.4 Couplings

The principal coupling effect results from the convection: a quantity of heat is transported by water, vapour and air flow. Vapour has a deep influence on the thermal balance and must be not neglected.

3. Mechanical behaviour modelling

In a clay barrier, the saturation and the suction can vary considerably. Research experiments have shown that the suction has a strong influence on the mechanical properties: the hardness and the shear strength of the soil increase with suction; the swelling or collapse can be induced; some irreversible deformations can even take place...
The mechanical behaviour modelling should be able to take this suction effect into account when the soil undergoes desaturation processes.

3.1 Stress state variables

The choice of stress state variables to describe the stress-strain relation is still an open question. Many researchers [4] have attempted to incorporate the suction s explicitly into an *effective stress* expression. For example, Bishop's postulate:

$$\sigma'_{ij} = \sigma_{ij} - p_g\,\delta_{ij} + \chi(p_g - p_w)\delta_{ij}. \tag{3.1}$$

Where σ'_{ij} is the effective stress tensor, σ_{ij} is the total stress tensor, χ represents the Bishop's coefficient which is a function of the saturation $S_{r,w}$, δ_{ij} refers to the Kronecker's tensor.
This concept presents some advantages: it is easy to implement into a finite element code [5], [6]; it provides qualitatively good predictions for problems involving mainly shear stresses...
But its application to modelling of the mechanical behaviour of unsaturated soils is limited mainly because of the following reasons:

1. Generally, the volumetric behaviour cannot be properly modelled with this postulate. In

particular, it is unable to model the collapse behaviour, which is a typical phenomenon of unsaturated soils during the wetting phase under certain external charges.

2. The Bishop's coefficient χ is a very complicate function. Experimental investigations [7] have shown that it may depend on the saturation $S_{r,w}$ but there is non-unique relation χ- $S_{r,w}$ for a given soil sample with different void ratios.
3. The value of χ is stress path dependant.
4. The experimental determination of χ is very difficult.

However, a simplified Bishop's postulate with $\chi=S_{r,w}$ has been implemented in the LAGAMINE code in order to model problems where the shear strain is dominant; it can be incorporated in any classical model (e.g. Drücker-Prager's model).
All these considerations lead to using the *independent stresses state variables* to model the mechanical behaviour of unsaturated soils. That is:

$$\begin{aligned} &\text{the net stresses tensor : } \sigma_{ij}^{*} = \sigma_{ij} - p_g \delta_{ij}, \\ &\text{the suction : } \qquad\qquad s = p_g - p_w. \end{aligned} \tag{3.2}$$

It is proved to be suitable for the modelling of the mechanical behaviour of unsaturated soils from the theoretical as well as the experimental points of view [8].

3.2 Alonso-Gens's mechanical model

The model proposed by Alonso et al [9] is based on the well-known CamClay model. It is written within the framework of the *independent stresses state variables* defined here above. In our finite element code *LAGAMINE*, the plastic yield surfaces are written in a three-dimensional stress space: $I_\sigma^* - II_{\hat{\sigma}}^* - s$ where I_σ^* is the first net stress invariant and $II_{\hat{\sigma}}^*$ refers to the second net deviatoric stress invariant.

3.2.1 The yield surfaces

The yield surface in the $I_\sigma^* - II_{\hat{\sigma}}^*$ space, named F_l, is written for a given value of suction as:

$$F_1 = \left(I_\sigma^{*2} + (I_0 - P_s) I_\sigma^* - I_0 P_s \right) \bar{r}^2 + II_{\hat{\sigma}}^{*2}. \tag{3.3}$$

Where $\bar{r}$ is defined as a *reduced radius* which represents the failure states and is given by:

$$\bar{r} = \frac{II_{\hat{\sigma}}}{I_\sigma} = C^{te} \quad \Rightarrow \quad \bar{r}_C = \bar{r}_E. \tag{3.4}$$

It can depend or not on the Lode's angle α, according to (Fig. 3.1):

$$\bar{r} = \begin{cases} C^{te}, & \text{Von - Mises} \\ a(1 + b * \sin 3\alpha)^n. & \text{Van - Eekelen} \end{cases} \tag{3.5}$$

a, b, n are constants which are linked to the internal friction angles in compression and extension; they may vary with the suction.
P_s represents the soil strength in extension, given by:

$$P_s = 3c / tg\phi_c. \tag{3.6}$$

Where c is the cohesion and ϕ_c refers to the internal friction angle in compression. Both c and ϕ_c may vary with suction; functions $c(s)$ and $\phi_c(s)$ based on experimental results can be introduced into the code.

I_0 represents the pre-consolidation of soil and varies with the suction (Fig. 3.2):

$$I_0 = p_c \left(\frac{I_0^*}{p_c}\right)^{\frac{\lambda(0)-\kappa}{\lambda(s)-\kappa}}. \tag{3.7}$$

Where I_0^* represents the pre-consolidation pressure of soil in saturated condition; p_c is a reference pressure; $\lambda(s)$ refers to the plastic slope of the compressibility curve against the net mean stress, it varies with the suction according to:

$$\lambda(s) = \lambda(0)\left[(1 - r)\exp(-\beta s) + r\right]. \tag{3.8}$$

Here $\lambda(0)$ is the plastic slope for the saturated condition. The elastic slope κ, of the compressibility curve against the net mean stress, may also be function of the suction. r and β are parameters describing the changes in soil stiffness with suction.

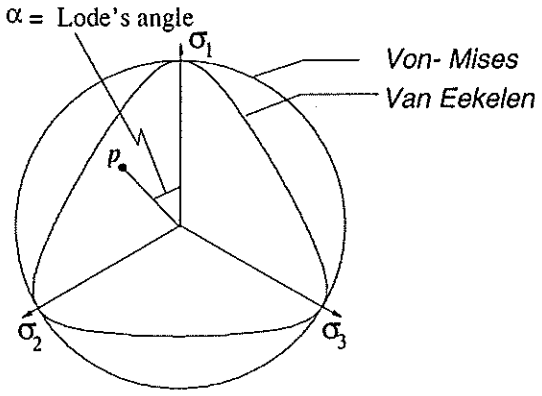

Figure 3.1: Yield surface - Lode's angle dependence

The yield surface (*SI*) in the $I_\sigma^* - s$ plane, named F_2, is given by (Fig. 3.2):

$$F_2 = s - s_0. \tag{3.9}$$

Where s_0 is a yield value, which represents the maximum, suction submitted by the soil.

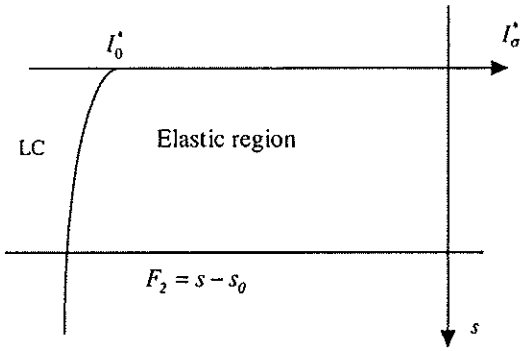

Figure 3.2. Yield surface in the $I_\sigma^* - s$ plane

The trace of the preconsolidation pressure in the $I_\sigma^* - s$ plane (equation 3.7) defines another part of the yield surface called LC (Loading Collapse) used for modelling the collapse behaviour under wetting.

3.2.2 Responses of the model

The elastic and plastic strains due to the stress (mechanical solicitations) are calculated by:

$$\dot{\sigma}_{ij}^e = C_{ijkl}^e \dot{\varepsilon}_{kl}^e. \text{ (Elastic deformations)} \tag{3.10}$$

$$\dot{\varepsilon}_{ij}^p = \dot{\lambda} \frac{\partial G}{\partial \sigma_{ij}}. \text{ (Plastic deformations)} \tag{3.11}$$

Where C_{ijkl}^e is the Hooke's tensor, $\dot{\sigma}_{ij}^e$ is the elastic net stress tensor, Q is the symbol for the plastic potential surface, and $\dot{\lambda}$ is obtained by the consistency condition.
A non-linear elasticity can be considered by means of:

$$\begin{aligned} K &= \frac{1+e}{3\kappa} I_\sigma^*, \\ G &= \frac{3(1-2\nu)}{2(1+\nu)} K. \end{aligned} \tag{3.12}$$

Where K is the soil bulk modulus, G its shear modulus, ν its Poisson's coefficient and e its void ratio.
A non-associated flow rule in the $I_\sigma^* - II_\sigma^*$ plane can be introduced into the model via the following equations:

$$\frac{\partial Q}{\partial II_{\hat{\sigma}}^*} = \eta \frac{\partial F}{\partial II_{\hat{\sigma}}^*}. \tag{3.13}$$

Where η is a parameter related to the $\vec{r}$, κ, and $\lambda(s)$.
The deformations induced by the suction change (hydric path) are:

$$\dot{\varepsilon}_{kl-s}^e = h^e \dot{s} \delta_{kl}. \text{ (Elastic deformations)} \tag{3.14}$$

$$\dot{\varepsilon}_{kl-s}^p = h^p \dot{s} \delta_{kl}. \text{ (Plastic deformations)} \tag{3.15}$$

With

$$h^e = \frac{\kappa_s}{3(1+e)(s+P_{at})}. \tag{3.16}$$

$$h^p = \frac{\lambda_s - \kappa_s}{3(1+e)(s+P_{at})}. \tag{3.17}$$

Where λ_s and κ_s are stiffness parameters for changes in suction and P_{at} is the atmospheric pressure. It should be noted that λ_s and κ_s could vary with the stress level.
The plastic deformation in compression due to the suction takes place when the suction is larger than s_0.
The elastic thermal dilatation is introduced in the model by:

$$\dot{\varepsilon}_{kl-T}^e = \xi \dot{T} \delta_{kl}. \tag{3.18}$$

Where ξ is the dilatation coefficient.
The evolution of yield surfaces is controlled by the total plastic volumetric strain ε_v^p developing in the soil via two state variables I_0^* and s_0:

$$dI_0^* = \frac{(1+e)I_0^*}{\lambda(0) - \kappa} d\varepsilon_v^p. \tag{3.19}$$

$$ds_0 = \frac{(1+e)(s_0 + P_{at})}{\lambda_s - \kappa_s} d\varepsilon_v^p. \tag{3.20}$$

After appropriate manipulations, the general constitutive relationship in reverse form can be written as:

$$\dot{\sigma}_{ij} = D_{ijkl} \dot{\varepsilon}_{kl} - V_{ij} \dot{s}. \tag{3.21}$$

Where D_{ijkl} is the classical elasto-plastic tensor and V_{ij} is a tensor related to the suction.

For the integration of the constitutive relation, we have used the so-called θ *point method*. To obtain more accurate results, the integration time step Δt is divided into N sub-steps dt. The sub-steps size can be automatically adjusted in function of the strain increment $\|\Delta\varepsilon\|$ or chosen by the user. For each sub-time step dt, the integration of equation (3.21) can be expressed as:

$$\begin{aligned} \sigma_{ij}(I+\theta dt) &= \sigma_{ij}(I) + \dot{\sigma}_{ij}(I).\theta.dt, \\ \sigma_{ij}(I+1) &= \sigma_{ij}(I) + \dot{\sigma}_{ij}(I+\theta dt).dt. \end{aligned} \tag{3.22}$$

Where I denotes the sub-time step number; θ is a numerical parameter that takes the value between 0 and 1 (usually $\theta > 0.5$ for reasons of numerical stability).
The hardening variables can be also integrated in the same way.
This version of the model can simulate the swelling and collapse behaviours but has some limitations for highly expansive materials: the plastic swelling deformation cannot be taken into account.

3.2.3 Sensitivity of the soil parameters

The parameters requested by the model and their determination means are outlined in table 3.1. Three series of suction controlled tests are required to determine the major parameters. The first one includes oedometer tests with wetting-drying cycles under different but constant vertical pressure. The second series consists of oedometer tests following several loading-unloading cycles under different but constant suctions. The third one should be a series of suctions controlled triaxial tests.
In practice, the determination of the parameters is not always evident. For example, the experimental results are not always easily interpreted; repeated tests do not always reproduce the same results. This throws doubt on the experimental results...
We should note that the yield surface LC governed by equation (3.7) is very sensitive and its convexity is not always guaranteed. Two difficulties are often met during calibration. Firstly we should avoid $\lambda(s) < \kappa$ in any cases. Secondly, the convexity of the LC is linked with the value of p_c; this latter is not easily determined directly from experimental results, we have to determine it by a calibration procedure. On the other hand, the LC calibration has an important influence on the model responses. We will show an example of validation tests to illustrate the difficulties during LC calibration.
In the case of non-linear elasticity, the shear module G depends on the Poisson's ratio ν and the stress level. From equation (3.12), we get:

$$G = \frac{3(1-2\nu)}{2(1+\nu)}\frac{(1+e)}{3\kappa}I_\sigma^* = \zeta\frac{(1+e)}{\kappa}I_\sigma^* \tag{3.23}$$

On figure 3.3, we have plotted the proportional coefficient ζ in function of ν.

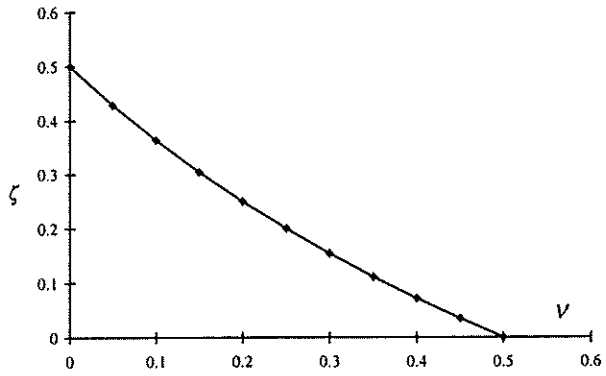

Figure 3.3 Influence of ν on the shear module of soil

We note that, for a given value of stress generated in the soil I_σ^*, the shear module G can decrease more than two times when ν changes from 0.3 to 0.4. However, the shear modulus G plays a most important role for generating the deviatoric stress which in turn control the hardening or softening aspects of the model responses.

Parameters	Determination means
e_0	Measured
$\lambda(0)$	Oedometer loading-unloading test in saturated state
I_0^*	Id.
λ_s	Oedometer or isotropic wetting-drying tests under different external charges.
κ_s	Id.
r	Series of suction controlled oedometer tests
β	Id.
p_c	Id. The measurements of I_0 at different level of suction are required to calibrate p_c
κ	Id. the function $\kappa(s)$ may be observed
C(s)	Series of suction controlled triaxial tests
$\varphi_c(s)$	Id.

Table 3.1. Parameters of the model

4. Validation test

The following modelling has been performed in the framework of a European Community research project entitled *Calculation and testing of behaviour of unsaturated clay (Catsius clay)*, to investigate both temperature and artificial hydration effects on the deformation and moisture transfer in the soil. The results of a small-scale wetting-heating test performed on highly compacted bentonite have been available [10]. The test has been performed inside a thermohydraulic cell, which is schematised in figure 4.1. The sample has been heated by means of the central heater and hydrated through the ports that are connected to the porous plate. During the test, the temperatures at different points, the volume of water flow and the swelling pressures generated in one point of the sample have been measured. The outer cell surface has been in contact with ambient air. The experience has elapsed during 2401.6 hours.
A finite element simulation is realised with the help of the developed finite elements with five-freedom degrees. The heating is modelled by imposing the temperature on the nodes of the sample in contact with the heater. The hydration procedure is modelled by increasing the water pressure on the nodes of porous plate. The convection transfer between the steel case and the ambient atmosphere is modelled thanks to the frontier thermal elements.
The steel case is supposed to be impermeable to the water flow. Both steel case and porous plate deformations are neglected. The system is initially at ambient temperature (293 °K). The gas pressure is supposed to remain fixed to the atmospheric pressure (100 kPa). The initial saturation of soil is 49% which gives an initial suction s =78.6 MPa according to the water retention curve.

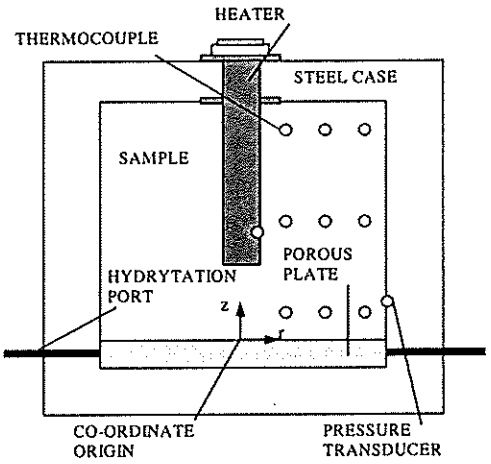

Figure 4.1: Configuration of the thermohydraulic cell

4.1 Finite element formulation

A bi-dimensional large strain finite element has been implemented in the finite element code

LAGAMINE. That element possesses five degrees of freedom at each node: two displacements of the soil skeleton, a liquid water pressure, a gas (dry air + vapour) pressure and a temperature. The number of nodes is variable (3,4,6 or 8) and the element is isoparametric, that's to say that the co-ordinates, velocities, pore pressure (water and gas) and temperature are discretised by the same shape functions.
We note a particularity of that element: if the description of the co-ordinates are parabolic, the spatial variation of the strains (spatial derivatives of the velocities) are thus linear, and in the same way the stresses (in elasticity). On the other hand, the variations of pore pressures and the temperature are parabolic, that's to say one degree higher than stresses. In some cases, that difference degree between stresses and pore pressure or temperature can provide numerical results less accurate. That is why, with that element, we have introduce the possibility to have a parabolic discretisation for the co-ordinates and the mechanics at the same time than a linear discretisation for the fluid (pore pressures and the temperature).
The thermo-hydro-mechanical coupling matrix is a monolithical one. The stiffness matrix in the Newton-Raphson sense of the coupled element is completely modified with regard to those corresponding to uncoupled elements. Indeed, for example concerning the coupling between mechanic and water pressure, we have to compute not only the displacements effect on nodal forces and the water pressure on nodal water flows, but also the water pressure effect on nodal forces (by way of the Terzaghi's postulate) and the displacements effects on nodal water flows (by way of the storage). Finally, in great transformations, we have to compute the effect of geometrical modifications on nodal water, gas and thermal flows. All coupling terms of the matrix are taken into account, providing a good convergence rate for most treated problems.
This stiffness matrix associates then five degrees of freedom per node and can been schematised as follow:

$$\underline{\underline{K}} = \begin{bmatrix} \underline{\underline{K}}_{MM} & \underline{\underline{K}}_{WM} & \underline{\underline{K}}_{GM} & \underline{\underline{K}}_{TM} \\ [2x2] & [2x1] & [2x1] & [2x1] \\ \underline{\underline{K}}_{MW} & \underline{\underline{K}}_{WW} & \underline{\underline{K}}_{GW} & \underline{\underline{K}}_{TW} \\ [1x2] & [1x1] & [1x1] & [1x1] \\ \underline{\underline{K}}_{MG} & \underline{\underline{K}}_{WG} & \underline{\underline{K}}_{GG} & \underline{\underline{K}}_{TG} \\ [1x2] & [1x1] & [1x1] & [1x1] \\ \underline{\underline{K}}_{MT} & \underline{\underline{K}}_{WT} & \underline{\underline{K}}_{GT} & \underline{\underline{K}}_{TT} \\ [1x2] & [1x1] & [1x1] & [1x1] \end{bmatrix} = \begin{bmatrix} \frac{\partial \underline{F}_M}{\partial \underline{x}_M} & \frac{\partial \underline{F}_M}{\partial p_w} & \frac{\partial \underline{F}_M}{\partial p_g} & \frac{\partial \underline{F}_M}{\partial T} \\ \frac{\partial \underline{F}_W}{\partial \underline{x}_M} & \frac{\partial \underline{F}_W}{\partial p_w} & \frac{\partial \underline{F}_W}{\partial p_g} & \frac{\partial \underline{F}_W}{\partial T} \\ \frac{\partial \underline{F}_G}{\partial \underline{x}_M} & \frac{\partial \underline{F}_G}{\partial p_w} & \frac{\partial \underline{F}_G}{\partial p_g} & \frac{\partial \underline{F}_G}{\partial T} \\ \frac{\partial \underline{F}_T}{\partial \underline{x}_M} & \frac{\partial \underline{F}_T}{\partial p_w} & \frac{\partial \underline{F}_T}{\partial p_g} & \frac{\partial \underline{F}_T}{\partial T} \end{bmatrix}$$

Figure 4.2: Stiffness matrix

Where $\underline{F}_M$ represents the nodal mechanical force, $\underline{F}_W$ the nodal water flux, $\underline{F}_G$ the nodal gas flux, $\underline{F}_T$ the nodal thermal flux, $\underline{x}_M$ the nodal displacements, p_w the nodal water pressure, p_g the nodal gas pressure and T the nodal temperature. The four mechanical, water flow, gas flow and thermal sub-matrixes, $\underline{\underline{K}}_{MM}$, $\underline{\underline{K}}_{WW}$, $\underline{\underline{K}}_{GG}$ and $\underline{\underline{K}}_{TT}$, are classical; all the others sub-matrixes

are coupling matrixes: for example, the two coupling sub-matrixes $\underline{K}_{MW}$ and $\underline{K}_{WM}$ represent respectively the coupling of mechanics onto water flow and water flow onto mechanics; the contribution of all theses coupling sub-matrixes is of first importance to obtain a good convergence, all the more their numerical evaluation is quite simple to perform.
Let's note also that to increase the numerical stability, the nodal water flows, gas flows and thermal flows, and the corresponding stiffness sub-matrixes, are always computed in the initial configuration.

4.2 Hydraulic and thermal properties

An equation describing the water retention curve is chosen to reproduce the measured data:

$$S_{r,w} = S_{r,res} + CSW3\frac{(S_{r,field} - S_{r,res})}{CSW3 + (CSW1.s)^{CSW2}}. \tag{4.1}$$

Where $S_{r,field}$ is the maximum saturation in the soil and $S_{r,res}$ is the residual saturation for a very high value of suction.

The water relative permeability is determined by:

$$\begin{aligned} k_{r,w} &= \frac{\left(S_{r,w} - S_{r,res}\right)^{CKW}}{\left(S_{r,field} - S_{r,res}\right)^{CKW}} \quad \text{if} \quad S_{r,w} \geq S_{r,res}, \\ k_{r,w} &= k_{r,w,\min} \qquad\qquad\quad \text{if} \quad S_{r,w} < S_{r,res}. \end{aligned} \tag{4.2}$$

The gas relative permeability is modelled by:

$$k_{r,g} = (1 - S_e)^{CKA1}.\left(1 - S_e{}^{CKA2}\right). \tag{4.3}$$

Where S_e is the effective saturation.

The water retention curve and the permeability are found to have an important influence on the water intake volume and the final saturation degree. The soil conductivity is a function of the saturation degree.

4.3 Parameters related to the mechanical model

The results of two series of suction controlled oedometer tests have been obtained to get the mechanical parameters [11, 12]. First one includes some tests with wetting-drying cycles under different constant vertical pressures. Another series of tests has been realised following several loading-unloading cycles under different constant suctions. By this way, the suction

yield parameter s_0 is obtained by the water retention curve.

4.4 Comparisons between simulation and experimental results

The figure 4.3 shows water intake evolution with time. A very good result is obtained: the experimental and numerical curves are almost the same.
The figure 4.4 shows the comparison between experimental and numerical result of the swelling pressure at the point with co-ordinates r=7.5 cm and z=1.25 cm during the experience. The agreement is good at the beginning, but decreases at the end of experience. In fact, the model didn't take into account some variations of certain parameters for this simulation, like κ_s varying with the net stress, κ depending on the suction, etc...

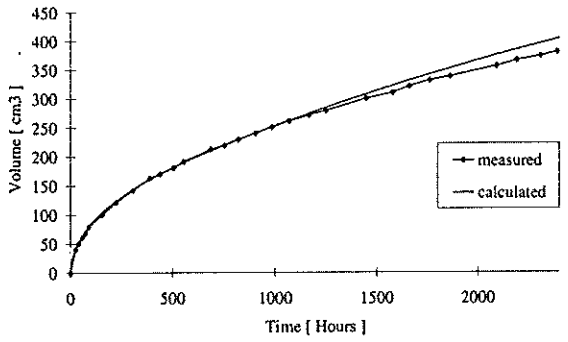

Figure 4.3: Water intake evolution

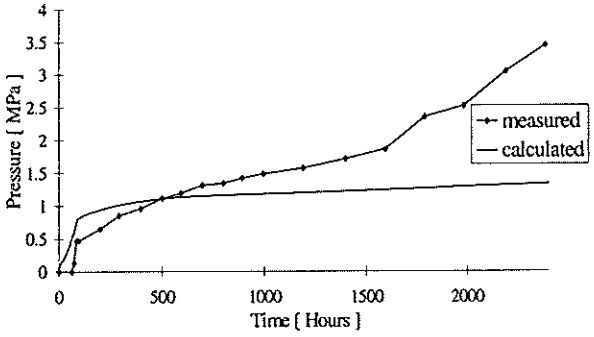

Figure 4.4: Swelling pressure evolution

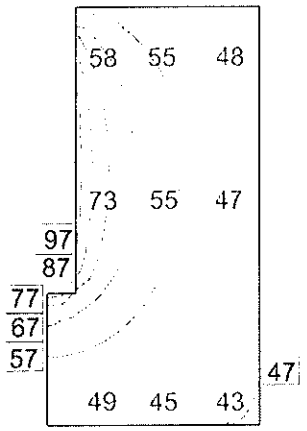

Figure 4.5: Temperature field at the end of experience

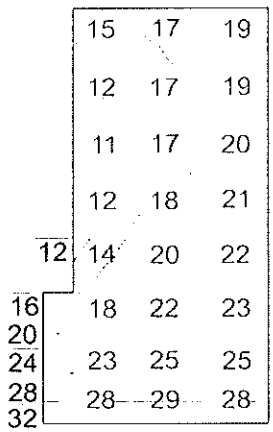

Figure 4.6: Water content at the end of experience

The calculated temperatures and water contents at the end of the experience are given in figure 4.5 and 4.6 respectively. The corresponding experimental measurements at some points

are also presented in grey on the same figure. The calculated temperatures are a little higher than the experimental ones. The numerical water content seems to be slightly lower than the experimental one at the analysed points. But they are close to the experimental ones near the heater. The generation of water vapour near the heater is a crucial phenomenon to take here into account. The vapour flow depends deeply on the temperature.
All the results appear to be very sensitive to the retention curve, the relative and intrinsic permeability.
A last remark could be that the soil mechanics has not a high influence on the water flow. Oppositely, the water flow has a deep influence on the mechanical behaviour.

4.5 Influence of the gas pressure

In the previous simulation, the gas pressure remains fixed to the atmospheric pressure. The (constant or variable) gas pressure effect has been checked thanks to simulations performed with (Case A) and without (Case B) a fixed gas pressure. In the case B, the steel case is supposed impermeable to gas. For both cases, the mechanical model is not taken into account. On the following pictures, the left part is the results of the case A and the right part of the case B.

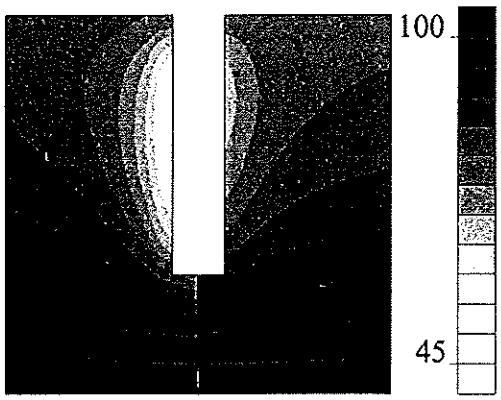

Figure 4.7: Saturation (%) at the end of the experiment

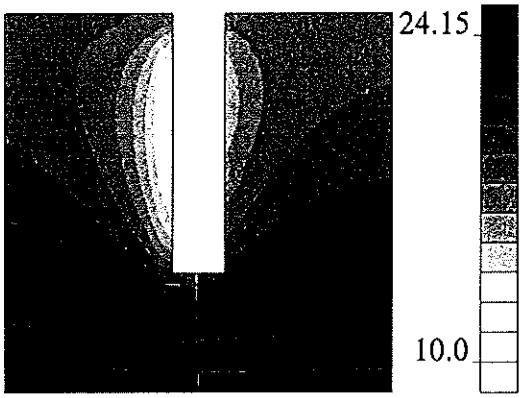

Figure 4.8: Water content (%) at the end of the experiment

The results show clearly differences between the two simulations. The saturation degree in case A varies from 47% to 100% while it varies from 62% to 100% in case B. In terms of suction, it means that the sample is submitted to a maximum suction of 85.1 MPa in case A and of 40.3 MPa in case B.
The computations have also shown that the gas pressure increases in a range from 302 kPa to 463 kPa.
This gas pressure increase should also have an influence on mechanical behaviour. Indeed, this increase modifies suction field and net stresses, which are the *independent variables* of the mechanical model.

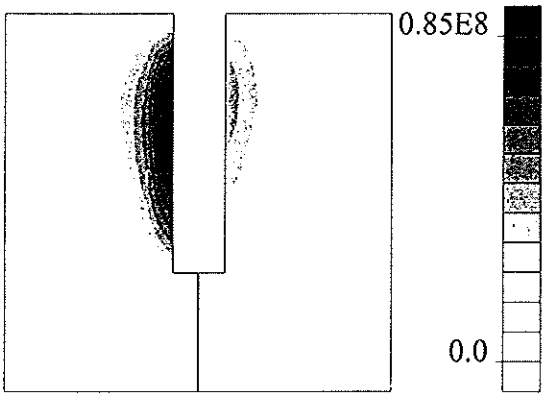

Figure 4.9: Suction (Pa) at the end of the experiment

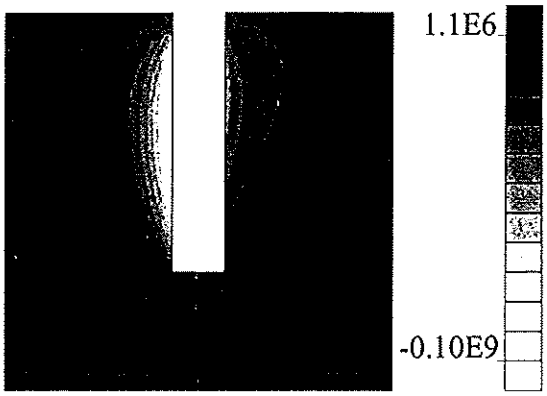

Figure 4.10: Water pressure (Pa) at the end of the experiment

4.6 Boundary condition and mass conservation

In the chosen formulation, balance equations are written for each species. Water specie is present in the liquid phase (liquid water) and in the gaseous phase (water vapour). Dry air is only present in the gaseous phase. Thus, the total water mass (liquid + vapour) and the dry air mass remain constant in the model.

On the figure 4.11 are drawn global water flows, liquid water flows and water vapour flows. As we write the balance equation of water specie, only the global water flows respect the boundary condition: no flows are allowed through the boundary as it is considered as impermeable to water.

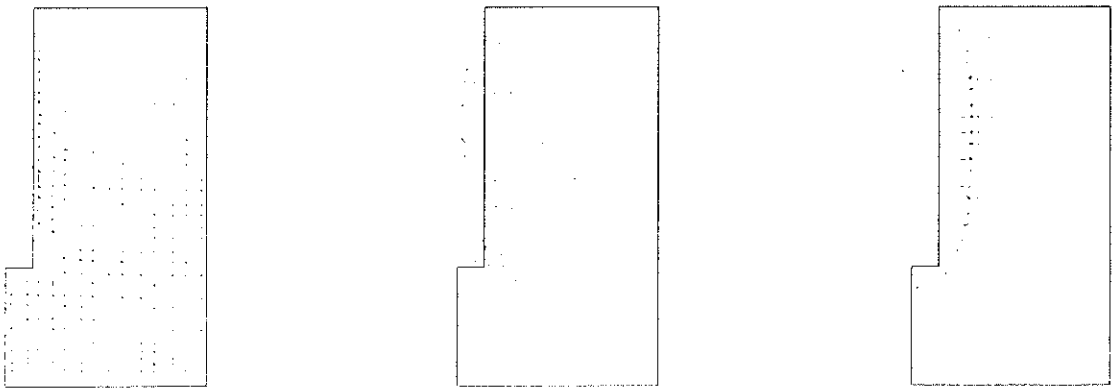

Figure 4.11: Water flows

However, the liquid flows and the vapour flows don't respect the boundary condition: this is a drawback of our formulation.
Other formulations could be developed with different combinations of degrees of freedom and different balance equations. The different possibilities are presented in the table 4.1.

Case	DOF	Balance equation	Boundary conditions respect	Pressure imposition
A	P_w	Liquid + vapour	Water flow	Water pressure
	P_g	Dry air	Dry air flow	Gas pressure
B	P_w	Liquid	Liquid water	Liquid pressure
	P_g	Dry air + vapour	Gas flow	Gas pressure
C	P_w	Liquid + vapour	Water flow	Water pressure
	P_a	Dry air	Dry air flow	Dry air pressure
D	P_w	Liquid	Liquid flow	Water pressure
	P_a	Dry air + vapour	Gas flow	Dry air pressure

Table 4.1

Let us discuss the different cases.

The results presented upper have been obtained with case A. Using a finite element with air pressure as degree of freedom (case C & D), it would be impossible to impose gas pressure. This choice is not perfectly convenient for the type of problems we care about.

The formulation with balance equations of liquid water and of gaseous phase (case B) allows that the liquid flows and the gas phase flows respect the boundary conditions. However, the vapour flows and the dry air flows don't respect them. In addition, in order to respect the global water mass conservation, the evaporation term must be computed and taken into account in the balance equation, what is not easy because state equations are based on equilibrium state.

In conclusion, each of the four formulations has drawback. The origin of the problem is the following. Water vapour characteristics (vapour pressure and vapour content) depend only on the temperature and the water and gas pressures. Thus, we cannot write a separated water vapour balance equation. Than, we must write a balance equation of a mixture (liquid + vapour or dry air + vapour). The boundary conditions will therefore be only respected by the mixture flows and not by each components flows.

5. CONCLUSION

A complete theory of a thermo-hydro-mechanical coupling model for unsaturated soils is provided in this paper. A validation test is performed to show the capabilities of the model to simulate the relevant phenomenon in nuclear energy storage. The comparison between simulation results and experimental ones is discussed. Some sensitivity of the mechanical parameters is also mentioned.

Acknowledgements

The authors thank the Europe Community for the support through the research project *Catsius clay* project. The support from FNRS is also greatly acknowledged.

References

[1] H.R. Thomas and Y. He: *Analysis of coupled heat, moisture and air transfer in a deformable unsaturated soil.* Géotechnique **45**, n°4, (1995), 677-689.

[2] N.E. Edlefsen and A.B.C. Anderson: *Thermodynamics of soils moisture.* Hilgardia **15**, n°2, (1943), 31-298.

[3] J.R. Philip and D.A. De Vries: *Moisture movement in porous materials under temperature gradients.* Trans. Am. Geophys. Un. **38**, (1957),222-232.

[4] A.W. Bishop and G.E. Blight: *Some aspects of effective stress in saturated and unsaturated soils.* Géotechnique n°**3**,(1963), 177-197.

[5] B.A. Schrefler, L. Simoni, X.K. Li and O.C. Zienkeiwicz: *Mechanics of partially saturated porous media.* In Numerical methods and constitutive modelling in geomechanics. C.S. Desai and G. Gioda, ed. CISM Courses and Lectures, N° **311**, Springer Verlag, (1990),169-209.

[6] R. Charlier and J.P. Radu: *Hydro-mechanical coupling and strain localisation.* Proc. NAFEMS World Congress, (1997).

[7] J.E.B. Jennings and J.B. Burland: *Limitations to the use of effective stresses in partly saturated soils.* Géotechnique **12**, n°2, (1962), 125-144.

[8] D.G. Fredlund and N.R. Morgenstern: *Stress state variables for unsaturated soils.* J. Geotech. Eng. Div. A.S.C.E. **103** GT5, (1977), 447-466.

[9] E.E. Alonso, A. Gens and A.A. Josa: *A constitutive model for partly saturated soil.* Géotechnique **40**, n°3, (1990), 405-430.

[10] CIEMAT REPORT. CEC Contract FI2W-CT91-0102 (DOEO). *Modelling and validation of the thermal-hydraulic-mechanical and geochemical behaviour of the clay barrier. Final report* 1991-1994. CIEMAT. DIRECCIÓN DE TECNOLOGÍA. TÉCNICAS GEOLÓGICAS. Madrid (1994).

[11] EUR REPORT, *Thermo-hydraulic-mechanical and geochemical behaviour of the clay barrier in radioactive waste repositories (model development and validation). Final report.* Directorate-General. Science, Research and Development, EUR 16744, EN. (1996).

[12] X.L. Li. *Comportement hydromécanique des sols fins : de l'état saturé à l'état non saturé.* Thèse de doctorat, MSM – Université de Liège, (1999).